




Article

Spontaneous Growth of $\text{CaBi}_4\text{Ti}_4\text{O}_{15}$ Piezoelectric Crystal Using Mixed Flux Agents

Mengdi Fan ¹, Guangda Wu ¹, Fapeng Yu ^{1,*}, Lili Li ¹, Yanlu Li ¹, Xiufeng Cheng ¹ and Xian Zhao ^{1,2,*}

¹ State Key Laboratory of Crystal Materials and Institute of Crystal Materials, Shandong University, Jinan 250100, China; fanmengdi950714@163.com (M.F.); wuguangda5@163.com (G.W.); 201511922@mail.sdu.edu.cn (L.L.); liyanlu@sdu.edu.cn (Y.L.); xfcheng@sdu.edu.cn (X.C.)

² Center for Optics Research and Engineering, Shandong University, Qingdao 266237, China

* Correspondence: fapengyu@sdu.edu.cn (F.Y.); xianzhao@sdu.edu.cn (X.Z.)

Received: 30 June 2020; Accepted: 10 August 2020; Published: 12 August 2020



Abstract: The bismuth layer-structured ferroelectrics (BLSFs) materials have potential for high-temperature piezoelectric applications. Among these piezoelectric materials, the $\text{CaBi}_4\text{Ti}_4\text{O}_{15}$ (CBT) piezoelectric ceramic with a high decomposition temperature of about 1250 °C attracts a lot of attention. Achieving a CBT single crystal is a significant way to improve its piezoelectric properties. For this purpose, the flux system for growing CBT crystal was explored in this study. The optimum flux composition ratio was found to be $\text{PbO}:\text{B}_2\text{O}_3:\text{CBT} = 3:3:1$ in mol%, where the $\text{PbO}-\text{B}_2\text{O}_3$ mixtures were used as a flux system. Millimeter size flake-shaped CBT crystals were obtained using the spontaneous growth process for the first time. The relationship between the crystal structure and flake growth habit was analyzed. In addition, the bandgap was evaluated by the combination of transmittance spectrum and first-principle calculations. Besides, the piezoelectric property was predicted from the perspective of polyhedral distortion, which indicated the potential of CBT crystal for piezoelectric applications.

Keywords: $\text{CaBi}_4\text{Ti}_4\text{O}_{15}$; single crystal growth; flux method; dipole moments

1. Introduction

Since the discovery of the piezoelectric effect, piezoelectric materials have been widely explored as sensors, transducers, actuators, energy harvesting devices, etc. Recently, piezoelectric materials that can maintain the electromechanical and piezoelectric properties at high temperatures and even harsh environments are needed, especially in aerospace industries, oil exploitation, and power plant fields [1–3]. The ever-increasing demands on operational temperature have stimulated a great deal of research effort on exploring piezoelectric materials with a high curie temperature (T_C) or high melting point, prior to which the electromechanical and piezoelectric properties should be maintained.

To date, several kinds of piezoelectric crystals with high melting points have been studied as the candidates for high-temperature piezoelectric applications [4–6]. For example, the modified langasite type crystal $\text{Ca}_3\text{Ta}(\text{Ga}_{1-x}\text{Al}_x)_3\text{Si}_2\text{O}_{14}$ (CTGAS) with a melting point above 1400 °C was determined to possess a relatively high piezoelectric coefficient ($d_{11} = 4.6$ pC/N) and electromechanical coupling factor ($k_{12} = 14.4\%$) [4]. The low-cost calcium aluminate silicate $\text{Ca}_2\text{Al}_2\text{SiO}_7$ (CAS) crystal with moderate piezoelectric activity was explored for high-temperature pressure sensing [5]. Furthermore, the $\text{RECa}_4\text{O}(\text{BO}_3)_3$ (ReCOB) crystals with good temperature stability and high electrical resistivity were studied for high-temperature vibration sensing applications [6]. Through the success fabrication of different prototypes of piezoelectric sensors, the sensitivity is expected to be further enhanced, which encourages the exploration of new piezoelectric crystals with strong piezoelectric response. Bismuth layer-structured

ferroelectrics (BLSFs), also known as Aurivillius-type ferroelectrics, have attracted much attention due to their strong piezoelectric response and ultrahigh Curie temperature T_C (600–900 °C). Among this type of piezoelectric material, the orthorhombic $\text{CaBi}_4\text{Ti}_4\text{O}_{15}$ (CBT) compound with a point group of 2 mm is believed to be a promising candidate for high-temperature piezoelectric applications, due to the merits of low electric conductivity, low dielectric loss, relatively large piezoelectric coefficient, and ease of fabrication by using the conventional solid-state reaction method [7–9]. However, the practical applications of CBT piezoelectric material at elevated temperatures are still restricted. The piezoelectric activity ($d_{33} = \sim 7$ pC/N) and stability need further improvement [10,11]. Many efforts have been made to improve the electromechanical and piezoelectric properties—for example, preparing the CBT-textured ceramics or conducting ion doping, etc. The piezoelectric coefficient d_{33} of CBT ceramics prepared by the reactive templated grain growth (RTGG) method with tape casting is reported to be as high as 45 pC/N [12]. However, the achieved improvement in piezoelectric activity for CBT ceramics has the problems of aging easily and grain boundaries. Single crystallization might be a good means to solve the above drawbacks and enhance the piezoelectric properties of CBT compounds. This strategy has been successfully performed on other piezoelectric ceramics. For example, $(\text{K}_{0.5}\text{Na}_{0.5})\text{NbO}_3$ (KNN) ceramics possessed a low piezoelectric coefficient $d_{33} < 100$ pC/N, while the piezoelectric coefficient of the KNN crystal reached about 150 pC/N [13,14].

It is of great significance to perform single crystallization for CBT ceramic and evaluate the electro-elastic properties for potential high-temperature piezoelectric applications. Since the CBT compound is incongruent and would decompose at temperature near 1250 °C, the flux method can be attempted to perform the single crystal growth. The flux method is a convenient, universal, and simple means to cultivate single crystals, and it has been widely used to grow various crystals with incongruent melting points, for example, KNN [14] and $\text{KBe}_2\text{BO}_3\text{F}_2$ (KBBF) crystals [15], etc. Although there have been extensive studies on the flux growth of functional crystal materials, the investigations on the single crystal growth of a CBT compound are very scarce [16], and the search for a suitable flux system for growing CBT single crystal is still on the way.

For this purpose, the flux systems suitable for CBT crystal growth were investigated. The CBT single crystals with dimensions up to millimeter size were grown for the first time using the $\text{PbO-B}_2\text{O}_3$ mixed flux agents. In addition, the relationship between crystal growth morphology and crystal structure was analyzed. The transmittance spectrum and the theoretical calculations of the CBT compound were reported, and the crystal polyhedral distortion and net dipole moment were discussed by theoretical calculation.

2. Materials and Methods

2.1. Polycrystalline Preparation

Prior to single crystal growth, the $\text{CaBi}_4\text{Ti}_4\text{O}_{15}$ polycrystalline compound was synthesized by a solid-state reaction method. High-purity CaCO_3 (4N, Alfa Aesar, Haverhill, MA, USA), Bi_2O_3 (4N, Aladdin, Shanghai, China), and TiO_2 (4N, Alfa Aesar, Haverhill, MA, USA) powders were selected as the starting raw materials, which were weighed according to the stoichiometric ratio. In order to compensate the evaporation of Bi_2O_3 during the solid-state reaction process, an excess amount of Bi_2O_3 (1 mol%) was added to the raw materials. For ensuing the synthesis of the CBT polycrystalline phase, we used two-step sintering. Firstly, all the raw materials were fully mixed, ground, and sintered at 800 °C for 10 h to decompose the CaCO_3 completely; then, they were ground again, pressed into cylindrical blocks, and sintered at 1000 °C for 20 h.

2.2. Flux Selection and Growth of CBT Crystal

According to the principle of selecting the flux agent, we studied the fluxing behaviors of two kinds of flux systems for crystallizing CBT crystal, i.e., Bi_2O_3 and $\text{PbO-B}_2\text{O}_3$ flux systems. The Bi_2O_3 and $\text{PbO-B}_2\text{O}_3$ flux systems have been successfully applied to the growth of other single crystals [16,17].

To avoid the introduction of impurities, we first consider the self-melting system. Hence, Bi_2O_3 was selected and used as the flux agent. The prepared CBT polycrystalline powders with the extra added Bi_2O_3 flux agent were mixed in different mole proportions ($\text{Bi}_2\text{O}_3\text{:CBT} = 3\text{:}1$, $4\text{:}1$ and $5\text{:}1$), heated, and melt at $1000\text{--}1100\text{ }^\circ\text{C}$ for 20 h and then slowly cooled down to room temperature. In addition to the Bi_2O_3 flux agent, $\text{PbO}\text{--}\text{Bi}_2\text{O}_3$ was chosen as the mixed flux system for crystallizing CBT crystal. PbO and Bi_2O_3 have their own merits for crystal growth using the flux method; reports indicate that PbO is an effective solvent used for many oxides and complex perovskites [18–24]. The Bi_2O_3 can reduce the melting temperature, increase the solubility of the melt, and create an optimum degree of complex formation and optimum viscosity [25]. Besides, because of its low melting point and high viscosity, Bi_2O_3 can also form a sealing layer to prevent the evaporation of PbO in the molten state at elevated temperatures. Based on the above considerations, the $\text{PbO}\text{--}\text{Bi}_2\text{O}_3$ mixed flux system was attempted for CBT single crystal growth. Firstly, the prepared CBT polycrystalline powders were mixed with the $\text{PbO}\text{--}\text{Bi}_2\text{O}_3$ flux systems in different mole proportions ($\text{PbO}\text{:}\text{Bi}_2\text{O}_3\text{:CBT} = 2\text{:}2\text{:}1$, $3\text{:}3\text{:}1$, $4\text{:}4\text{:}1$, $5\text{:}1\text{:}1$, and $5\text{:}3\text{:}1$) to perform the comparative experiments. Secondly, the mixed compounds were heated and melt at $1000\text{--}1100\text{ }^\circ\text{C}$ for 20 h; then, they were slowly cooled down to room temperature to find the expected crystal phase.

In this study, the CBT crystal was finally grown by the spontaneous nucleation method using $\text{PbO}\text{--}\text{Bi}_2\text{O}_3$ as flux. The CBT polycrystalline powders, high-purity PbO (4N, Aladdin, Shanghai, China) and Bi_2O_3 (4N, Alfa Aesar, Haverhill, MA, USA), were weighed in a certain mole proportion (the proportion for CBT and $\text{PbO}\text{--}\text{Bi}_2\text{O}_3$ mixed flux was $\text{PbO}\text{:}\text{Bi}_2\text{O}_3\text{:CBT} = 3\text{:}3\text{:}1$). The powders were mixed thoroughly, ground, and placed into platinum crucibles in a growth furnace, after which the crucible was slowly heated to $1000\text{ }^\circ\text{C}$ and maintained at this temperature for 20 h to make the solution melt completely and mix homogeneously. After that, the crucible was cooled slowly to $500\text{ }^\circ\text{C}$ with a very low rate of $2\text{--}5\text{ }^\circ\text{C/h}$ and then to room temperature at $10\text{ }^\circ\text{C/h}$. When the spontaneous crystallization process was finished, the crucible was boiled with nitric acid to separate the flux from the crystallized CBT crystals.

2.3. Transmission Spectra Measurement and Phase Characterization

The transmission spectra of polycrystalline CBT were measured with a Nicolet IS 10 (Thermo Fisher, Waltham, MA, USA) over the wavelength range of 400 to 4000 nm at room temperature. The crystal phase of the solidified CBT solution obtained by using different flux systems and different proportions was identified by using the Bruker AXS D8 Advance X-ray diffractometer (XRPD, Bruker-axs, Karlsruhe, Germany) at room temperature.

2.4. Theoretical Calculations

The band structure calculations of CBT compound employed the Vienna ab initio Simulation Package (VASP 5.3.5) [26,27] implementation of density functional theory (DFT) in conjunction with the projector-augmented wave (PAW) [28] method. Thereby, the $\text{Ca } 4s^2$, $\text{Bi } 6s^2 6p^3$, $\text{Ti } 3d^2 4s^2$, and $\text{O } 2s^2 2p^4$ states were treated as valence electrons. The electronic wave functions were expanded in plane waves using an energy cutoff of 400 eV. The electron exchange and correlation (XC) within the General Gradient Approximation (GGA) of the Perdew, Burke, and Ernzerhof (PBE) [29] functional was used to optimize the configurations, and the force convergence criterion for the structural relaxation was set to 0.01 eV/\AA . The electronic properties were performed by the screened hybrid functional of Heyd, Scuseria, and Ernzerhof (HSE06) [30,31]. $4 \times 4 \times 4$ and $2 \times 2 \times 2$ Monkhorst-Pack [32] k -point meshes were employed to sample the Brillouin zones for PBE and HSE06 calculations, respectively.

3. Results and Discussion

3.1. XRPD Analysis and Crystallization

The polycrystalline CBT compounds were synthesized in a stoichiometric ratio with an excess amount of Bi_2O_3 (1 mol%) added for compensating the evaporation of Bi_2O_3 during the solid-state

reaction process. There were individual impurity peaks (TiO_2 component) observed in the compounds obtained by sintering the stoichiometric raw materials using the solid-state reaction method, as shown in Figure 1a. In addition, experimental results proved that the CBT crystalline phase was difficult to obtain solely using Bi_2O_3 or PbO as flux agents. When using Bi_2O_3 as the flux agent ($\text{Bi}_2\text{O}_3\text{:CBT} = 3\text{:}1$, $4\text{:}1$ and $5\text{:}1$), the main compound was $\text{Bi}_{12}\text{Ti}_{20}\text{O}_{20}$, and no CBT phase was detected using XRPD (Figure 1b). Similarly, when using PbO as the flux agent ($\text{PbO:CBT} = 2\text{:}1$, $3\text{:}1$ and $4\text{:}1$), the impurity phase is mainly $\text{Pb}_x\text{Bi}_y\text{Ti}_z\text{O}_{(2x+3y+4z)/2}$ ($x, y, z \geq 0$) compounds (Figure 1c). In contrast, when using the mixed $\text{PbO-Bi}_2\text{O}_3$ flux system and selecting the ratio of $\text{PbO:Bi}_2\text{O}_3$ to be $1\text{:}1$, the CBT single crystal phase could be achieved. However, when the ratio deviated from $1\text{:}1$, the impurity phases such as the $\text{Pb}_5\text{B}_8\text{O}_{17}$ and $\text{Bi}_{12}\text{Ti}_{20}\text{O}_{20}$ might be formed, as presented in Figure 1d.

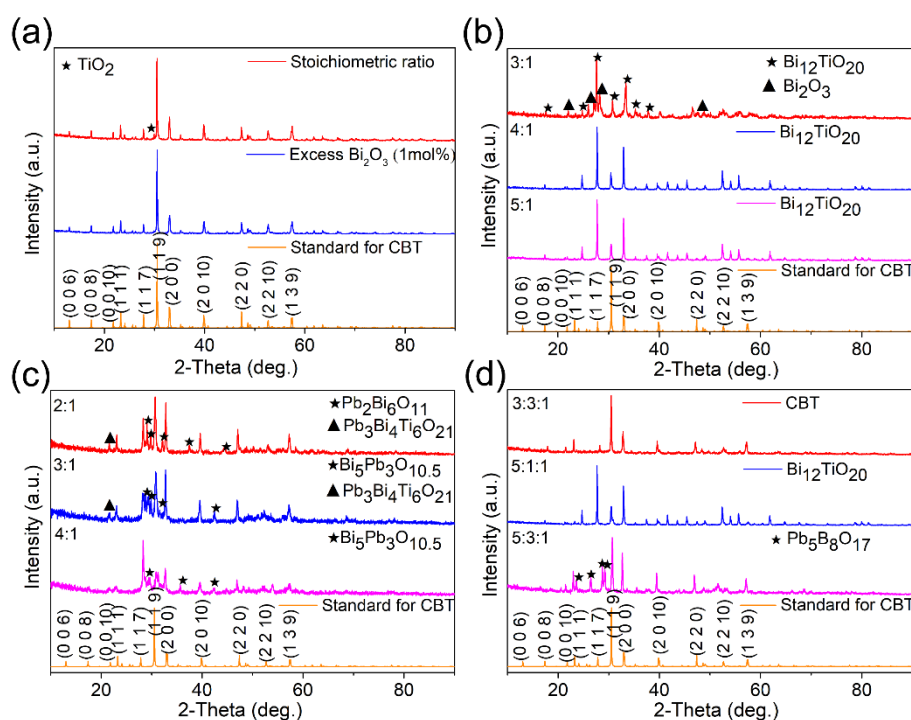


Figure 1. X-ray diffractometer (XRPD) patterns of the crystalline $\text{CaBi}_4\text{Ti}_4\text{O}_{15}$ (CBT) compounds: (a) XRPD pattern of the synthesized polycrystalline powder; (b) XRPD pattern of the polycrystalline using Bi_2O_3 as flux; (c) XRPD pattern of the polycrystalline using PbO as flux; (d) XRPD pattern of polycrystalline using $\text{PbO-Bi}_2\text{O}_3$ as flux.

Considering that the $\text{PbBi}_4\text{Ti}_4\text{O}_{15}$ (PBT) compound has the same symmetry with CBT crystal, further XRPD analysis was performed to identify the crystalline CBT phase. Figure 2a gives the XRPD patterns of crystalline CBT with different flux ratios and compared with the PBT phase. It is observed that the diffraction angle of the main peak at approximately 30.54° for CBT is higher than that of PBT (ICSD No.173544). However, the main peaks in the patterns of crystalline CBT with different flux ratios ($\text{PbO:Bi}_2\text{O}_3\text{:CBT} = 2\text{:}2\text{:}1$, $3\text{:}3\text{:}1$ and $4\text{:}4\text{:}1$) are kept the same with standard CBT (ICSD No. 99500), supporting that the obtained crystal phase is CBT rather than PBT. Experimental results indicate that when the flux ratio is $2\text{:}2\text{:}1$, the mixed compounds are difficult to solute, while when the ratio is $4\text{:}4\text{:}1$, the solubility is relatively low. Therefore, the optimum flux ratio was obtained to be $\text{PbO:Bi}_2\text{O}_3\text{:CBT} = 3\text{:}3\text{:}1$. In order to evaluate the purity of crystalline CBT compounds obtained by using the mixed $\text{PbO-Bi}_2\text{O}_3$ flux agents ($\text{PbO:Bi}_2\text{O}_3\text{:CBT} = 3\text{:}3\text{:}1$), the refined crystal structure by the Rietveld method for the powder X-ray diffraction was performed. Results are shown in Figure 2b. It is indicated that the differences between the pristine data and the refined data are very small, showing a good agreement with the measurements.

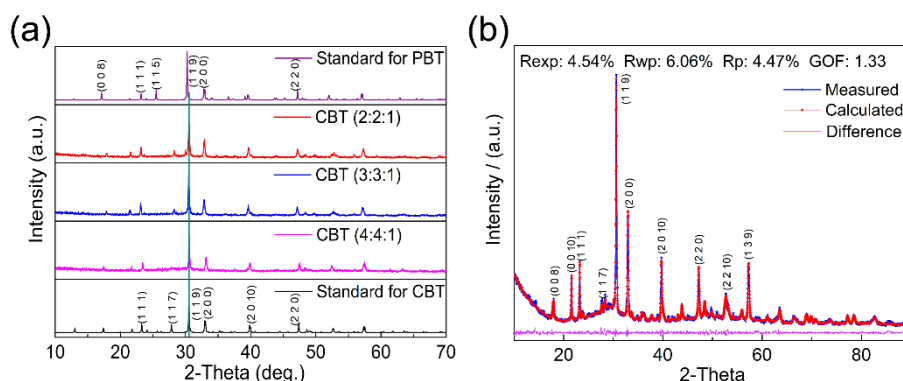


Figure 2. (a) XRPD patterns of crystalline CBT with different flux ratios ($\text{PbO}:\text{B}_2\text{O}_3:\text{CBT} = 2:2:1, 3:3:1,$ and $4:4:1$) and compared with the $\text{PbBi}_4\text{Ti}_4\text{O}_{15}$ (PBT) phase; (b) XRPD patterns of crystalline CBT compounds obtained after refinement.

The CBT single crystals with millimeter dimensions were successfully grown by using the spontaneous nucleation process using the mixed $\text{PbO}-\text{B}_2\text{O}_3$ flux agents ($\text{PbO}:\text{B}_2\text{O}_3:\text{CBT} = 3:3:1$). The crystalline state in the platinum crucible and the photographs of as-grown flake-shaped CBT crystals are shown in Figure 3a,b, respectively.

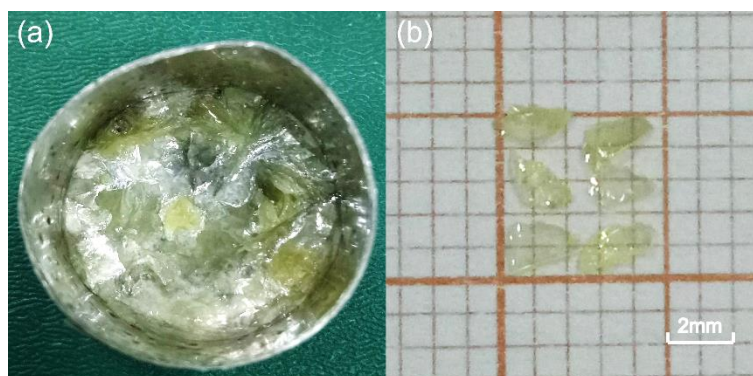


Figure 3. (a) Top-view of the as-cooled Pt crucible showing the grown CBT crystals by spontaneous nucleation process; (b) Selected flake-shaped CBT crystals crystallized from mixed flux agents ($\text{PbO}:\text{B}_2\text{O}_3:\text{CBT} = 3:3:1$).

3.2. Structure–Morphology Relationships

The crystal structures of the four-layer ferroelectric Aurivillius phases $\text{ABi}_4\text{Ti}_4\text{O}_{15}$ ($A = \text{Ca}, \text{Sr}, \text{Ba},$ and Pb) were reported by B.J. Kennedy et al. [33], but they lack descriptions in detail about the CBT crystal with a bismuth-layered structure. The relationship between the crystal structure and morphology was analyzed based on the refined structure data by the Rietveld method. The results are shown in Figure 4. The CBT crystal structure is composed of Bi_2O_2 layers and TiO_6 octahedrons arranged alternately along the crystallographic c -axis, where $0.6\text{Bi}(2)/0.4\text{Ca}(1)$ and $0.7\text{Bi}(3)/0.3\text{Ca}(3)$ atoms are occupied in the intervals among TiO_6 octahedrons. The flake-shaped morphology is closely related to the bismuth layer structure of CBT crystal. It is believed that the flake-shaped morphology is associated with the Bi_2O_2 layer in the CBT crystal. Generally speaking, the bonding strength decreases with the increase of bond length, and large bond lengths are easy to break. It is found that the bond distance of the $\text{Bi}(1)-\text{O}$ is about 2.55 \AA and 2.69 \AA , which is much longer than that of the $\text{Ti}-\text{O}$ bond (1.77 \AA and 1.89 \AA), as presented at Figure 4b. Therefore, the CBT crystal is relatively difficult to grow along the crystallographic c -axis due to the weak chemical bonding, but it is relatively easy to grow along the a - and b -axes. In addition, it is found that the axis ratio c/a for CBT crystal reached 7.5065,

exhibiting strong structural anisotropy. There are the reasons why the CBT crystal grown along the crystallographic c -axis shows a flake growth habit.

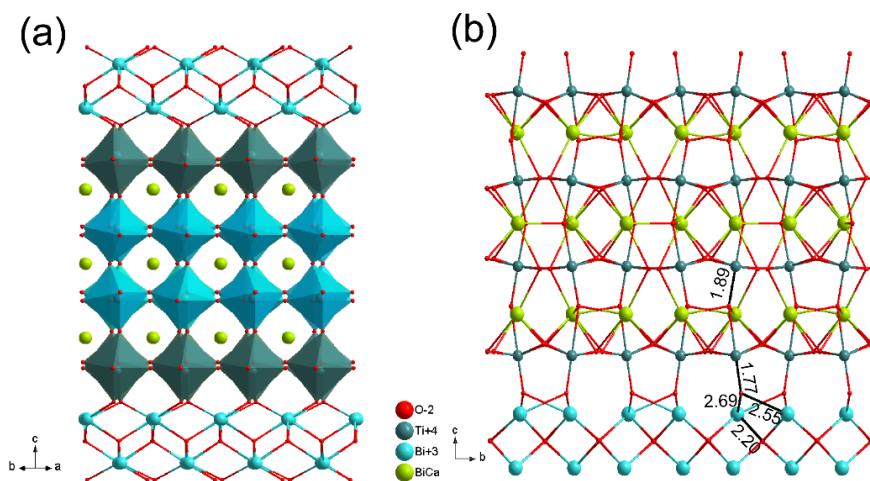


Figure 4. Schematic crystal structure of the $\text{CaBi}_4\text{Ti}_4\text{O}_{15}$ crystal: (a) projected along the $[110]$ direction; (b) projected along the crystallographic a -axis in space (the unit in Å).

3.3. Piezoelectric Activity Evaluation

$\text{CaBi}_4\text{Ti}_4\text{O}_{15}$ crystal belongs to the 2 mm point group; thus, it has a non-centrosymmetric structure, which determines that the CBT crystal has piezoelectric properties. In order to explore its potential applications in piezoelectric fields, preliminary evaluations were conducted.

3.3.1. Transmission Spectra

For high-temperature piezoelectric application, the electrical conductivity is an important factor that influences the dielectric loss and temperature stability of the electro-elastic properties. Usually, the electrical conductivity at high temperatures is associated with the bandgap. In this study, the transmittance for CBT polycrystalline sample was measured at room temperature, and the band structure was calculated. As shown in Figure 5, the transmittance from 910 to 4000 nm is about 90% and gradually decreases below the wavelength of 910 nm and reaches zero at about 400 nm, indicating that the transmission cut-off edge of the CBT is about 400 nm, which corresponds to the bandgap of 3.11 eV and is very close to calculated bandgap 3.17 eV. These results are basically consistent with the value reported by Tanwar et al. (3.36 eV) [34].

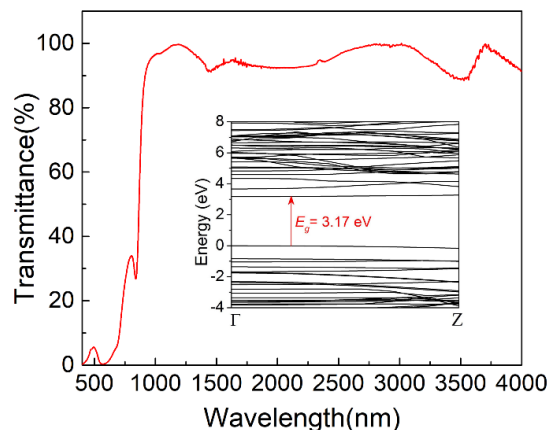


Figure 5. The transmittance spectrum of the prepared polycrystalline CBT powders measured at room temperature (inset shows the calculated band structure).

3.3.2. Dipole Moment Calculation

The piezoelectric activity is closely related to the polyhedron distortion and net dipole moment. As for the polyhedron distortion in CBT crystal, there are several types of polyhedron distortions (Figure 6a), among which the distortion Δd for Bi(1)O₆ octahedron was calculated by using the following formula [35]:

$$\Delta d = \frac{\|(\text{Bi}-\text{O1})\| - \|(\text{Bi}-\text{O4})\|}{|\cos \theta_1|} + \frac{\|(\text{Bi}-\text{O2})\| - \|(\text{Bi}-\text{O5})\|}{|\cos \theta_2|} + \frac{\|(\text{Bi}-\text{O3})\| - \|(\text{Bi}-\text{O6})\|}{|\cos \theta_3|} \quad (1)$$

where the O1–O6 are coordination oxygen atoms of the Bi(1)O₆ octahedron, and θ_1 , θ_2 , and θ_3 are bond angles. The distortion Δd for the Bi(1)O₆ octahedron was found to be 1.37 Å, which can be identified as strong distortions according to the fourth category defined by Halasyamani [35]. Generally, the larger the polyhedron distortion, the stronger the piezoelectric activity of the crystals. Besides the polyhedron distortion, the net dipole moments in CBT crystal were studied, according to the bond-valence theory [36–40].

Table 1 summarizes the dipole moments of each polyhedron in CBT crystal. It was found that the magnitude of the net dipole moment in the unit cell of the CBT crystal was about 37 Debye, which is comparable with the α -BiB₃O₆ single crystal (35 Debye), of which the piezoelectric charge coefficient d_{22} was determined to be in the order of 40 pC/N [41]. Additionally, the directions of the dipole moment for the polyhedral and unit cell of the CBT crystal are identified and shown in Figure 6b, where the net dipole moment direction of the CBT unit cell was negative along the crystallographic *c*-axis. The calculated results indicated that the Bi(1)O₆ octahedron showed a larger distortion and contributed to the piezoelectric activity of the CBT crystal. Hence, it is predicted that the CBT single crystal has excellent piezoelectric performances.

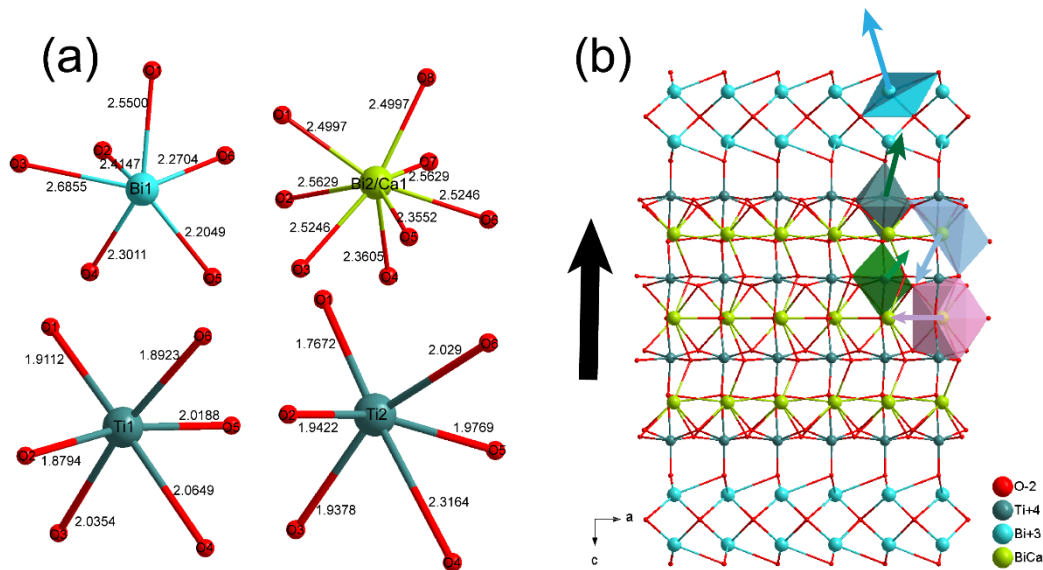


Figure 6. (a) Structural distortions for MO₆ octahedron in the CBT crystal (M represents Bi, Ca, and Ti atoms); (b) Directions of the dipole moment in the polyhedral and unit cell of CBT crystal (the black arrow indicates the net dipole moment).

Table 1. Dipole moments calculated for CBT single crystal.

Crystal	Species	Δd (Å)	Dipole Moments				
			x (a)	y (b)	z (c)	Debye	$\times 10^{-4}$ edu·cm/Å ³
CBT *	Bi(1)O6	1.37	−2.0168	−6.7630	−14.5406	16.16	541.46
	Ca(1)/Bi(2)O8	0.60	−9.9685	−0.1447	0	9.97	333.99
	Ca(3)/Bi(3)O7	-	−8.2239	3.3904	10.8491	14.03	470.00
	Ti(1)O6	0.44	4.3457	0.0852	−2.8455	5.20	174.04
	Ti(2)O6	0.69	2.3948	−0.5329	−8.4905	8.84	296.07
	Unit cell	-	0	0	−37.35	−37.35	−312.78

* The crystallographic data of CBT was derived from the refined structure by the Rietveld method.

4. Conclusions

In summary, the flake-shaped CBT crystals in the millimeter range were grown by the flux method using the mixed PbO–B₂O₃ agents for the first time. The optimum flux composition mole ratio was found to be PbO:B₂O₃:CBT = 3:3:1. The flake-shaped growth habit of the CBT crystal was analyzed from the perspective of a microcrystal structure. The structural distortions and the net dipole moment of the CBT crystal were found to be 1.37 Å (Bi(1)O₆ octahedron) and 37 Debye, respectively. The Bi(1)O₆ octahedron showed the larger distortion and believed to contribute to the piezoelectric activity of the CBT crystal. In addition, the transmittance spectrum of the CBT crystal was measured and found to show a broad transmission range, where the bandgap was found to be near 3.11 eV. However, the main problem encountered in CBT growth is the observed flake growth habit. In the following studies, the large-size single crystal growth by using the top-seeded method with mixed PbO–B₂O₃ fluxes will be performed.

Author Contributions: Conceptualization, M.F. and F.Y.; methodology, M.F., L.L., Y.L. and X.C.; validation, F.Y., X.Z.; investigation, M.F. and G.W.; resources, F.Y. and X.Z.; writing—original draft preparation, M.F.; writing—review and editing, F.Y. All authors have read and agreed to the published version of the manuscript.

Funding: This work was supported by The Key Research and Development Program of Shandong Province (Nos.2017CXGC0413 and 2019JZZY010313), and the National Natural Science Foundation of China (No. 51872165).

Conflicts of Interest: The authors declare no conflict of interest.

References

1. Zhang, S.J.; Yu, F.P. Piezoelectric materials for high temperature sensors. *J. Am. Ceram. Soc.* **2011**, *94*, 3153–3170. [\[CrossRef\]](#)
2. Jiang, X.N.; Kim, K.; Zhang, S.J.; Johnson, J.; Salazar, G. High-temperature piezoelectric sensing. *Sensors* **2014**, *14*, 144–169. [\[CrossRef\]](#) [\[PubMed\]](#)
3. Wu, J.G.; Gao, X.Y.; Chen, J.G.; Wang, C.M.; Zhang, S.J.; Dong, S.X. Review of high temperature piezoelectric materials, devices, and applications. *Acta Phys. Sin.* **2018**, *67*, 207701.
4. Yokota, Y.; Ohashi, Y.; Kudo, T.; Kochurikhin, V.V.; Medvedev, A.; Kurosawa, S.; Kamada, K.; Yoshikawa, A. Effects of Al Substitution for Ca₃Ta(Ga_{1-x}Al_x)₃Si₂O₁₄ Piezoelectric Single Crystals. *J. Cryst. Growth* **2017**, *468*, 321–325. [\[CrossRef\]](#)
5. Hagiwara, M.; Noguchi, H.; Hoshina, T.; Takeda, H.; Fujihara, S.; Kodama, N.; Tsurumi, T. Growth and Characterization of Ca₂Al₂SiO₇ Piezoelectric Single Crystals for High-Temperature Sensor Applications. *Jpn. J. Appl. Phys.* **2013**, *52*, 09KD03. [\[CrossRef\]](#)
6. Zhang, S.J.; Fei, Y.T.; Frantz, E.; Snyder, D.W.; Chai, B.H.T.; Shrout, T.R. High-Temperature Piezoelectric Single Crystal ReCa₄O(BO₃)₃ for Sensor Applications. *IEEE Trans. Ultrason. Ferroelectr. Freq. Control* **2008**, *55*, 2703–2708. [\[CrossRef\]](#)
7. Zheng, L.Y.; Li, G.R.; Zhang, W.Z.; Yin, Q.R. The Structure and Properties of Bi-Layered Piezoelectric Ceramics Bi₄(Ca, Sr)Ti₄O₁₅. *Jpn. J. Appl. Phys.* **2002**, *41*, L1471–L1473. [\[CrossRef\]](#)

8. Yan, H.X.; Li, C.E.; Zhou, J.G.; Zhu, W.M.; He, L.X.; Song, Y.X.; Yu, Y.H. Effects of A-Site (NaCe) Substitution with Na-Deficiency on Structures and Properties of $\text{CaBi}_4\text{Ti}_4\text{O}_{15}$ -Based High-Curie-Temperature Ceramics. *Jpn. J. Appl. Phys.* **2001**, *40*, 6501–6505. [\[CrossRef\]](#)
9. Subbarao, E.C. A Family of Ferroelectric Bismuth Compounds. *J. Phys. Chem. Solids* **1962**, *23*, 665–676. [\[CrossRef\]](#)
10. Khokhar, A.; Mahesh, M.L.V.; James, A.R.; Goyal, P.K.; Sreenivas, K. Sintering Characteristics and Electrical Properties of $\text{BaBi}_4\text{Ti}_4\text{O}_{15}$ Ferroelectric Ceramics. *J. Alloy. Compd.* **2013**, *581*, 150–159. [\[CrossRef\]](#)
11. Zhou, Z.Y.; Li, Y.C.; Hui, S.P.; Dong, X.L. Effect of Tungsten Doping in Bismuth-Layered $\text{Na}_{0.5}\text{Bi}_{2.5}\text{Nb}_2\text{O}_9$ High Temperature Piezoceramics. *Appl. Phys. Lett.* **2014**, *104*, 012904. [\[CrossRef\]](#)
12. Takeuchi, T.; Tani, T.; Saito, Y. Piezoelectric Properties of Bismuth Layer-Structured Ferroelectric Ceramics with a Preferred Orientation Processed by the Reactive Templated Grain Growth Method. *Jpn. J. Appl. Phys.* **1999**, *38*, 5553–5556. [\[CrossRef\]](#)
13. Jaeger, R.E.; Egerton, L. Hot Pressing of Potassium-Sodium Niobates. *J. Am. Ceram. Soc.* **1962**, *45*, 209–213. [\[CrossRef\]](#)
14. Lin, D.B.; Li, Z.R.; Zhang, S.J.; Xu, Z.; Yao, X. Dielectric/Piezoelectric Properties and Temperature Dependence of Domain Structure Evolution in Lead Free $(\text{K}_{0.5}\text{Na}_{0.5})\text{NbO}_3$ single crystal. *Solid State Commun.* **2009**, *149*, 1646–1649. [\[CrossRef\]](#)
15. Tang, D.Y.; Xia, Y.N.; Wu, B.C.; Chen, C.T. Growth of A New UV Nonlinear Optical Crystal: $\text{KBe}_2(\text{BO}_3)\text{F}_2$. *J. Cryst. Growth* **2001**, *222*, 125–129. [\[CrossRef\]](#)
16. Tellier, T.; Boullay, P.; Manier, M.; Mercurio, D. A Comparative Study of the Aurivillius Phase Ferroelectrics $\text{CaBi}_4\text{Ti}_4\text{O}_{15}$ and $\text{BaBi}_4\text{Ti}_4\text{O}_{15}$. *J. Solid State Chem.* **2004**, *177*, 1829–1837. [\[CrossRef\]](#)
17. Dong, M.; Ye, Z.G. High-Temperature Solution Growth and Characterization of the Piezo-/Ferroelectric $(1-x)\text{Pb}(\text{Mg}_{1/3}\text{Nb}_{2/3})\text{O}_3$ - $x\text{PbTiO}_3$ [PMNT] single crystals. *J. Cryst. Growth* **2000**, *209*, 81–90. [\[CrossRef\]](#)
18. Saitoh, S.; Takeuchi, T.; Kobayashi, T.; Harada, K.; Shimanuki, S.; Yamashita, Y. An Improved Phased Array Ultrasonic Probe Using $0.91\text{Pb}(\text{Zn}_{1/3}\text{Nb}_{2/3})\text{O}_3$ - 0.09PbTiO_3 Single Crystal. *Jpn. J. Appl. Phys.* **1999**, *38*, 3380–3384. [\[CrossRef\]](#)
19. Yamashita, Y.; Shimanuki, S. Synthesis of Lead Scandium Niobate-Lead Titanate Pseudo Binary System Single Crystals. *Mater. Res. Bull.* **1996**, *31*, 887–895. [\[CrossRef\]](#)
20. Brunskill, I.H.; Boutellier, R.; Depmeier, W.; Schmid, H. High-Temperature Solution Growth of $\text{Pb}(\text{Fe}_{0.5}\text{Nb}_{0.5})\text{O}_3$ and $\text{Pb}(\text{Mn}_{0.5}\text{Nb}_{0.5})\text{O}_3$ Crystals. *J. Cryst. Growth* **1982**, *56*, 541–546. [\[CrossRef\]](#)
21. Brixel, W.; Boutellier, R.; Schmid, H. Flux Growth and Characterization of Single Crystals of the Perovskites $\text{Pb}_2\text{FeTaO}_6$ and Pb_2CoWO_6 . *J. Cryst. Growth* **1987**, *82*, 396–404. [\[CrossRef\]](#)
22. Ye, Z.G.; Tissot, P.; Schmid, H. Pseudo-Binary $\text{Pb}(\text{Mg}_{1/3}\text{Nb}_{2/3})\text{O}_3$ - PbO Phase Diagram and Crystal Growth of $\text{Pb}(\text{Mg}_{1/3}\text{Nb}_{2/3})\text{O}_3$ [PMN]. *Mater. Res. Bull.* **1990**, *25*, 739–748. [\[CrossRef\]](#)
23. Sun, B.N.; Boutellier, R.; Sciau, P.; Burkhardt, E.; Rodriguez, V.; Schmid, H. High Temperature Solution Growth of Perovskite Pb_2CoWO_6 Single Crystals. *J. Cryst. Growth* **1991**, *112*, 71–83. [\[CrossRef\]](#)
24. Ye, Z.G.; Schmid, H. Growth From High Temperature Solution and Characterization of $\text{Pb}(\text{Fe}_{2/3}\text{W}_{1/3})\text{O}_3$ Single Crystals. *J. Cryst. Growth* **1996**, *167*, 628–637. [\[CrossRef\]](#)
25. Elwell, D.; Sheel, H.J. *Crystal Growth from High Temperature Solution*, 3rd ed.; Academic Press: New York, NY, USA, 1975; pp. 94–95.
26. Kresse, G.; Furthmüller, J. Efficiency of ab-initio Total Energy Calculations for Metals and Semiconductors Using a Plane-Wave Basis Set. *Comput. Mater. Sci.* **1996**, *6*, 15–50. [\[CrossRef\]](#)
27. Kresse, G.; Furthmüller, J. Efficient Iterative Schemes for ab initio Total-Energy Calculations Using a Plane-Wave Basis Set. *Phys. Rev. B* **1996**, *54*, 11169–11186. [\[CrossRef\]](#)
28. Kresse, G.; Joubert, D. From ultrasoft pseudopotentials to the projector augmented-wave method. *Phys. Rev. B* **1999**, *59*, 1758–1775. [\[CrossRef\]](#)
29. Perdew, J.P.; Burke, K.; Ernzerhof, M. Generalized Gradient Approximation Made Simple. *Phys. Rev. Lett.* **1996**, *77*, 3865–3868. [\[CrossRef\]](#)
30. Heyd, J.; Scuseria, G.E.; Ernzerhof, M. Hybrid functionals based on a screened Coulomb potential. *J. Chem. Phys.* **2003**, *118*, 8207–8215. [\[CrossRef\]](#)
31. Krukau, A.V.; Vydrov, O.A.; Izmaylov, A.F.; Scuseria, G.E. Influence of the exchange screening parameter on the performance of screened hybrid functionals. *J. Chem. Phys.* **2006**, *125*, 224106. [\[CrossRef\]](#)

32. Monkhorst, H.J.; Pack, J.D. Special Points for Brillouin-Zone Integrations. *Phys. Rev. B* **1976**, *13*, 5188–5192. [[CrossRef](#)]
33. Kennedy, B.J.; Zhou, Q.D.; Ismunandar; Kubota, Y.; Kato, K. Cation Disorder and Phase Transitions in the Four-Layer Ferroelectric Aurivillius Phases $\text{ABi}_4\text{Ti}_4\text{O}_{15}$ ($\text{A} = \text{Ca}, \text{Sr}, \text{Ba}, \text{Pb}$). *J. Solid State Chem.* **2008**, *181*, 1377–1386. [[CrossRef](#)]
34. Tanwar, A.; Sreenivas, K.; Gupta, V. Effect of Orthorhombic Distortion on Dielectric and Piezoelectric Properties of $\text{CaBi}_4\text{Ti}_4\text{O}_{15}$ Ceramics. *J. Appl. Phys.* **2009**, *105*, 084105. [[CrossRef](#)]
35. Halasyamani, P.S. Asymmetric Cation Coordination in Oxide Materials: Influence of Lone-Pair Cations on the Intra-Octahedral Distortion in d^0 Transition Metals. *Chem. Mater.* **2004**, *16*, 3586–3592. [[CrossRef](#)]
36. Brese, N.E.; O’Keeffe, M. Bond-Valence Parameters for Solids. *Acta Cryst. B* **1991**, *47*, 192–197. [[CrossRef](#)]
37. Ok, K.M.; Halasyamani, P.S. Mixed-Metal Tellurites: Synthesis, Structure, and Characterization of $\text{Na}_{1.4}\text{Nb}_3\text{Te}_{4.9}\text{O}_{18}$ and $\text{NaNb}_3\text{Te}_4\text{O}_{16}$. *Inorg. Chem.* **2005**, *44*, 3919–3925. [[CrossRef](#)]
38. Maggard, P.A.; Nault, T.S.; Stern, C.L.; Poeppelmeier, K.R. Alignment of Acentric $\text{MoO}_3\text{F}_3^{3-}$ Anions in a Polar Material: $(\text{Ag}_3\text{MoO}_3\text{F}_3)(\text{Ag}_3\text{MoO}_4)\text{Cl}$. *J. Solid State Chem.* **2003**, *175*, 27–33. [[CrossRef](#)]
39. Izumi, H.K.; Kirsch, J.E.; Stern, C.L.; Poeppelmeier, K.R. Examining the Out-of-Center Distortion in the $[\text{NbOF}_5]^{2-}$ Anion. *Inorg. Chem.* **2005**, *44*, 884–895. [[CrossRef](#)]
40. Kim, J.H.; Halasyamani, P.S. A Rare Multi-Coordinate Tellurite, $\text{NH}_4\text{ATe}_4\text{O}_9 \cdot 2\text{H}_2\text{O}$ ($\text{A} = \text{Rb}$ or Cs): The Occurrence of TeO_3 , TeO_4 , and TeO_5 Polyhedra in the Same Material. *J. Solid State Chem.* **2008**, *181*, 2108–2112. [[CrossRef](#)]
41. Chen, F.F.; Jiang, C.; Tian, S.W.; Yu, F.P.; Cheng, X.F.; Duan, X.L.; Wang, Z.P.; Zhao, X. Electroelastic Features of Piezoelectric $\text{Bi}_2\text{ZnB}_2\text{O}_7$ Crystal. *Cryst. Growth Des.* **2018**, *18*, 3988–3996. [[CrossRef](#)]



© 2020 by the authors. Licensee MDPI, Basel, Switzerland. This article is an open access article distributed under the terms and conditions of the Creative Commons Attribution (CC BY) license (<http://creativecommons.org/licenses/by/4.0/>).